



**HAL**  
open science

## Determination of concrete water content by coupling electromagnetic methods: Coaxial/cylindrical transition line with capacitive probes

Géraldine Villain, Amine Ihamouten, Xavier Derobert

► **To cite this version:**

Géraldine Villain, Amine Ihamouten, Xavier Derobert. Determination of concrete water content by coupling electromagnetic methods: Coaxial/cylindrical transition line with capacitive probes. *NDT & E International*, 2017, 88, pp.59-70. 10.1016/j.ndteint.2017.02.004 . hal-01592882v2

**HAL Id: hal-01592882**

**<https://hal.science/hal-01592882v2>**

Submitted on 28 Sep 2017

**HAL** is a multi-disciplinary open access archive for the deposit and dissemination of scientific research documents, whether they are published or not. The documents may come from teaching and research institutions in France or abroad, or from public or private research centers.

L'archive ouverte pluridisciplinaire **HAL**, est destinée au dépôt et à la diffusion de documents scientifiques de niveau recherche, publiés ou non, émanant des établissements d'enseignement et de recherche français ou étrangers, des laboratoires publics ou privés.

1 **Determination of concrete water content**  
2 **by coupling electromagnetic methods: Coaxial/cylindrical**  
3 **transition line with capacitive probes**

4 Géraldine VILLAIN<sup>(1)</sup>, Amine IHAMOUTEN<sup>(2)</sup>, Xavier DEROBERT<sup>(1)</sup>

5  
6 <sup>(1)</sup> Université Bretagne-Loire, IFSTTAR Site of Nantes, Allée des Ponts et Chaussées, CS4, F-44344  
7 Bouguenais, France

8 <sup>(2)</sup> CEREMA, DTO/DLRCA, ERA17-CND, Angers, France

9 [geraldine.villain@ifsttar.fr](mailto:geraldine.villain@ifsttar.fr), [amine.ihamouten@cerema.fr](mailto:amine.ihamouten@cerema.fr), [xavier.derobert@ifsttar.fr](mailto:xavier.derobert@ifsttar.fr)

10 \*corresponding author, e-mail adress: [geraldine.villain@ifsttar.fr](mailto:geraldine.villain@ifsttar.fr), tel: 33 2 40 84 5722

11

12 **Abstract**

13 This paper deals with the development and the validation of an innovative, easy-to-use and on  
14 site technique for determination of concrete water content. The on-site technique is the  
15 capacitive probe, able to characterize in situ dielectric media in the 30-35 MHz frequency  
16 band (around 33 MHz). For the evaluation of water content in various civil engineering  
17 structures, a calibration methodology has to be developed and is presented herein. It is based  
18 on the complex permittivity estimation of various dispersive concretes, which is carried out  
19 by a cylindrical coaxial electromagnetic (EM) transition line allowing the characterization in  
20 laboratory of material samples in a large GPR frequency bandwidth [50-600 MHz]. This  
21 methodology consists then on a coupling between the results of both the capacitive probes and  
22 the coaxial EM cell extrapolated at low frequency (33 MHz). The extrapolation procedure  
23 used to link physically the results of the two techniques is provided by the 4p-variant of  
24 Jonscher's model which is parameterized to obtain dispersion curves of the complex  
25 permittivity for very wide frequency bands. The methodology is checked by a parametric  
26 study that associates the 4p variant of Jonscher's model with the physical and hydric  
27 characteristics of the six concrete mix designs representing high performance and ordinary  
28 concretes at various hydric states. The surface testing results measured by capacitive probes  
29 on slabs are successfully compared to the extrapolated results obtained on cores.

30

31 **Keywords**

32 Durability; diagnosis; saturation degree; reinforced concrete; dielectric constant;  
33 permittivity; dispersion curves.

34

## 35 Highlights

- 36 • Methodology to get calibration curve linking water content and permittivity;
- 37 • Jonscher's model used to fit dispersion curves of complex permittivity;
- 38 • Experimental campaign on 6 various concretes at 4 water contents;
- 39 • Analysis of the results obtained by 2 electromagnetic NDT methods;
- 40 • Validation of the methodology coupling the 2 NDT methods.

41

## 42 1. Introduction

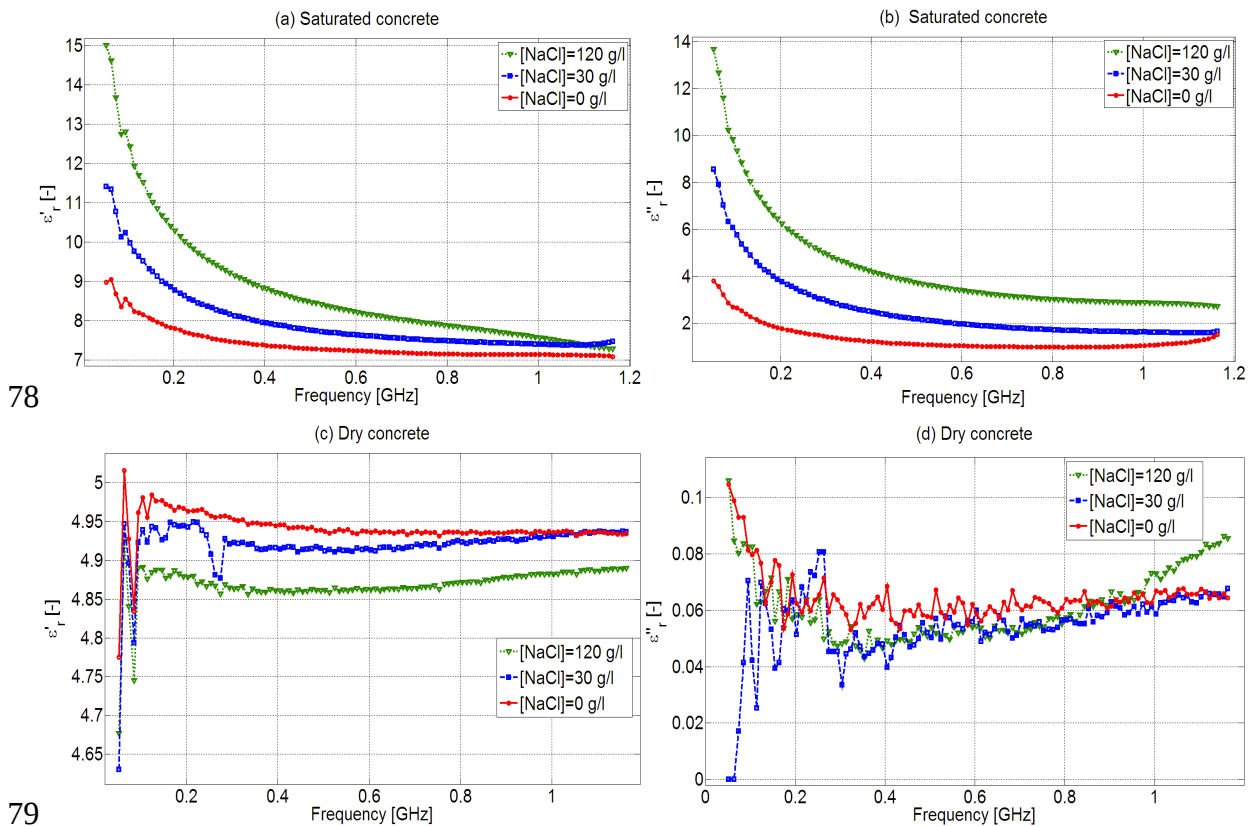
43 It is essential to determine the concrete water content of a reinforced concrete structure  
44 in the context of sustainable structural preservation. Water content is namely a key factor,  
45 first, to perform a diagnosis on concrete conditions and durability performances and, then, to  
46 predict the residual service life of the studied reinforced concrete structure [1]. The non-  
47 destructive testing (NDT) methods based on electromagnetic (EM) wave propagation are very  
48 sensitive to the water content of concrete on the one hand and sensitive to the nature of the  
49 mixing components (limestone or siliceous aggregates, cement, silica fume, blast furnace slag,  
50 fly ash...) on the second hand [2-9]. Thereby, non-destructive testing techniques based on EM  
51 wave propagation constitute a valuable means for monitoring the condition of concrete. For  
52 non-magnetic materials, the wave propagation is entirely governed by their complex effective  
53 permittivity, which reflects the interaction between propagating EM waves and the tested  
54 material including the solid matrix and the porosity filled by air and by interstitial solution  
55 containing different ions.

56 For this purpose, several techniques have been developed, with varying degrees of  
57 success, in order to describe the frequency dependence of the dielectric permittivity of  
58 geological and civil engineering materials [8-17]. This frequency dependence of complex  
59 permittivity has introduced the notion of material dispersion [18, 19]. Generally speaking, EM  
60 characterization measurements, done on a conductive dielectric, give a complex effective  
61 permittivity  $\epsilon^*_e$ , which encompass the polarization effects, characterized by atomic or  
62 orientation polarizability, and the migration of free charge carriers that are ions and electrons.  
63 Moreover, its frequency dependence reflects different polarization and conduction  
64 mechanisms potentially related to the inherent material properties. For most of such  
65 literature, the relative permittivity  $\epsilon^*_r$ , defined by the ratio  $\epsilon^*_e/\epsilon_0$  (where  $\epsilon_0$  is the permittivity  
66 of free space), is used while defining the dielectric constant as the real part  $\epsilon'_r$ , and the tangent

69 loss  $\tan \delta = \epsilon''_r / \epsilon'_r$ . In the following, studies will be focused on  $\epsilon'_r$  and  $\epsilon''_r$  under the generic  
 70 term dielectric permittivity.

71 Recent researches [8, 15, 17, 21] demonstrated the dependence of the complex  
 72 permittivity to the water and chloride contents in concrete (Fig. 1) with a discrimination  
 73 between the two effects according to the frequency bandwidth and the nature of the  
 74 observable (real or imaginary part of the permittivity). In the example of Fig. 1, it is possible  
 75 to quantify the effect produced by the presence of chloride ions in the range of very low  
 76 frequencies.

77



78

79

80 Figure 1: Frequency variation of the complex relative permittivity at various chloride contents for a concrete  
 81 with  $W/C=0.5$  and siliceous aggregates (C2) -a-b- Real and imaginary parts at the saturated state -c-d- Real and  
 82 imaginary parts at the dried state [22].

83

84

85 Unfortunately, using conventional methods for determining the dielectric properties of  
 86 concrete in different conditions becomes not sufficient. As the evaluation of the water content  
 87 is one of the main factors of the penetration of aggressive agents in concrete, thus, of the  
 88 evolution of the durability of reinforced concrete structures, the study focuses on the  
 89 volumetric water content of concrete.

90

91In this paper, we propose a methodology to evaluate the water content of concrete structures.  
92The principle is based on the assessment of the complex permittivity carried out on a large  
93frequency bandwidth. The methodology consists first on a coupling between the results of  
94capacitive probes, able to characterize in situ dielectric media in the 30-35 MHz frequency  
95band (around 33 MHz), and the ones of a coaxial/cylindrical transition line (also named EM  
96cell). This EM cell enables to characterize material samples in the range [50 MHz - 600 MHz]  
97in laboratory. The equations of the fitting dispersion curves are provided by the 4p variant of  
98Jonscher's model [11, 16]. Moreover, it is shown here that the dispersion curves can be  
99extrapolated on very wide frequency band [30-2000 MHz]. Thus, for each studied concrete  
100mix design, a calibration curve linking the permittivity at 33 MHz with the water content can  
101be established. It can then be used to transform the capacitive probes measurements into  
102concrete water content. In the same way and in the same time, the dispersion curves can be  
103used at high frequency corresponding to GPR to build the calibrations curves. The last will  
104serve for subsequent nondestructive in situ investigation by ground penetrating radar (GPR).  
105The whole methodology is validated thanks to a parametric study that associates the 4p-  
106variant of Jonscher's model with the physical and hydric characteristics of six concretes with  
107various mix designs representing high performance concretes, ordinary concretes and very  
108porous concretes at various volumetric water contents.

109

110In the following Section II, the capacitive technique for on-site NDT evaluation of concrete  
111structure conditions and the coaxial/cylindrical transition line used in the laboratory for  
112calibration are presented. Then, in Section III, the general principle behind complex  
113permittivity estimation in a wide bandwidth using the 4p-variant of Jonscher's model  
114extrapolation will be described and validated on published data. In Section IV, the  
115experimental protocol is summarized. Section V is devoted to the analysis of the validation  
116results.. Lastly, conclusions are drawn in Section VI.

117

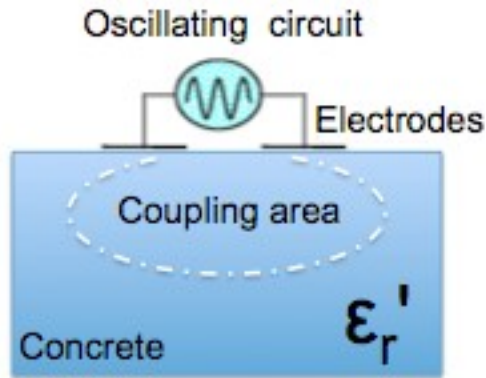
## 118**2. The electromagnetic techniques used in this study**

119

### 120**2.1. Capacitive probes**

121The principle of capacitive measurements is based on the calculation of the resonance  
122frequency of an oscillating AC electric circuit (around 30-35 MHz) between the electrodes  
123(Fig. 2), which are in contact with the upper face of the tested medium [23, 24].

124



125

a)

b)

126 Figure 2: Capacitive probes -a- Schematic principle diagram -b- Photo of the device including several electrode  
127 sets.

128

129 This system forms a planar capacitor where the change in the capacitance  $C$  (F) is indicative  
130 of the dielectric nature of the medium components (*i.e.* the nature and the size of the  
131 aggregates, the water content, the chloride content ...). The change in the value of this  
132 capacitance involves a variation in the resonance frequency of the system  $f_{osc}$  following the  
133 relation:

$$134 \quad f_{osc} = \frac{1}{2\pi\sqrt{LC}} = \frac{1}{2\pi\sqrt{LK_{geo}\epsilon'_r}} \quad (1)$$

135

136 where  $L$  (H) is the system inductance,  $K_{geo}$  a geometric constant and  $\epsilon'_r$  the real part of the  
137 relative equivalent permittivity of the coupling medium.

138

139 The volume investigated by the capacitive probes is highly dependent on the geometry of the  
140 electrodes. Four sets of electrodes (investigation depths equal to 2-3 mm for the small-size  
141 electrodes named PE, 2-3 cm for the medium-size ME and 8 cm for great-size electrodes GE  
142 which are stable, 5-6 cm for the set 3E which is optional and not stable) informs on the  
143 presence of any gradient according to depth. This device has been used to determine water  
144 content gradients in concrete [20, 21, 25]. It has also been adapted to study the filling of post-  
145 tension duct with cementitious grouts [26].

146 Considering equation (1), the relationship between  $f_{osc}$  and  $\varepsilon'_r$  can be effective only from the  
 147 determination of the own system parameters. Obtaining these parameters is made via a probe  
 148 calibrating protocol using standard materials.

149

### 150 Calibrating protocol

151 The objective of this calibrating protocol is to determine the parameters necessary for  
 152 calculating the system capacitance from its resonance frequency  $f_{osc}$ , using slabs of standard  
 153 materials (PVC, Teflon, marble, granite, limestone and eccostock) where the dielectric  
 154 properties are well known. Equation (1) can be reformulated as:

$$155 \quad f_{osc} = \frac{l}{2\pi\sqrt{L(C_{mat} + C_{probe})}} = \frac{l}{2\pi\sqrt{LC_{probe}\left(1 + \frac{C_{mat}}{C_{probe}}\right)}} \quad (2)$$

156 In the case of civil engineering materials, we can admit that  $C_{mat} \ll C_{probe}$ .

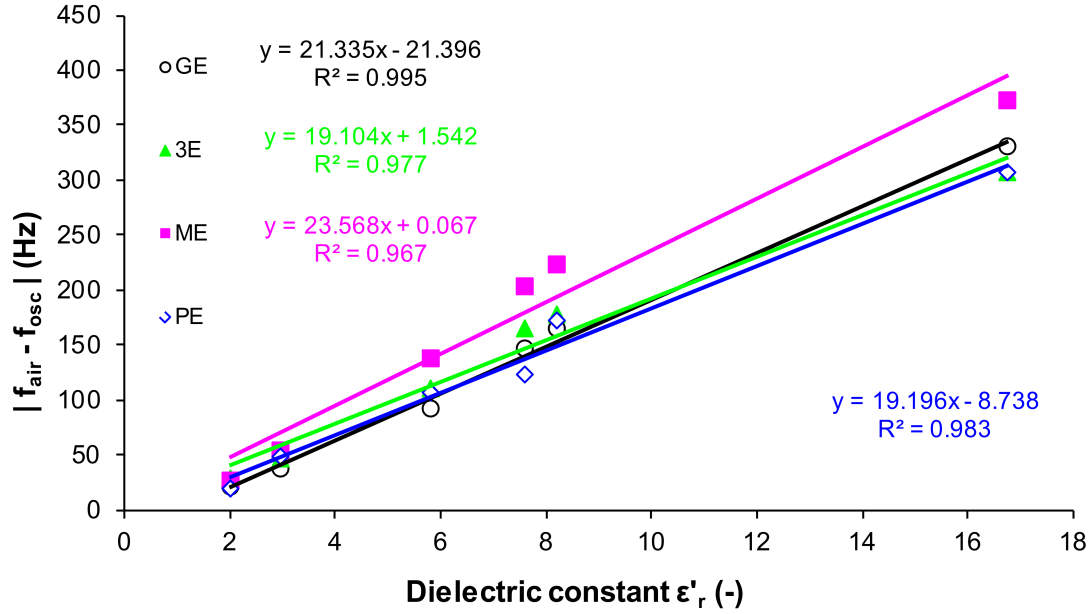
157 Following this, we perform an order 2 Taylor expansion of the function  $f_{osc}$  according to the  
 158 variable  $C_{mat}/C_{probe}$ , which gives us:

$$159 \quad f_{osc} = A - \frac{A}{2} \frac{C_{mat}}{C_{probe}} \quad \text{where} \quad A = \frac{l}{2\pi\sqrt{LC_{probe}}} \quad (3)$$

160

161 This equation shows that the relationship between  $C_{mat}/C_{probe}$  and  $f_{osc}$  is linear. To reduce the  
 162 interference effects due to the external environment of the system (temperature and humidity),  
 163 the calibrating protocol requires a measurement in air  $f_{air}$  before any test on standard  
 164 materials. Figure 3 shows the results for all the electrode sets. The values of the relative  
 165 permittivity real part of standard materials are obtained via the EM cell measurements at  
 166 100 MHz.

167



168

169 Figure 3: Results from the calibrating protocol of capacitive probes: oscillating frequency difference  $|f_{air} - f_{osc}|$  vs  
 170 the real part of the relative permittivity of standard materials.

171

172 For transposing the results expressed as real relative permittivity to results expressed  
 173 as reference capacitance, we use equation (1). The determination of the geometrical parameter  
 174  $K_{geo}$  was performed by numerical modeling on Femlab® (developed by Comsol®) [14]. The  
 175 results of this modeling are given in Table 1.

176

177 Table 1: Estimation of the geometrical parameter  $K_{geo}$  for various materials.

| Material  | Dimensions<br>(mm <sup>3</sup> ) | Dielectric<br>constant (-) | $K_{geo}$ [-] |       |       |
|-----------|----------------------------------|----------------------------|---------------|-------|-------|
|           |                                  |                            | GE            | ME    | PE    |
| Concrete  | 200×200×60                       |                            | 1.077         | 1.007 | 1.005 |
| PTFE      | 200×200×60                       | 2                          | 0.923         | 0.975 | 0.991 |
| PVC       | 200×200×60                       | 2.95                       | 0.923         | 0.975 | 0.991 |
| Granite   | 600×600×153                      | 5.8                        | 1.0           | 1.0   | 1.0   |
| Marble    | 300×300×100                      | 7.6                        | 1.011         | 1.008 | 1.0   |
| Limestone | 300×300×80                       | 8.2                        | 1.02          | 1.004 | 0.996 |
| Eccostock | 200×200×60                       | 16.75                      | 0.923         | 0.975 | 0.991 |

178

179 The determination of the coefficient  $A = -80,6$  pF in equation (2) is carried out by identifying  
 180 the coefficients of the linear regression of the oscillation frequency difference  $|f_{air} - f_{osc}|$  as  
 181 function of the permittivity. These results obtained on standard materials confirm those  
 182 obtained on electronic circuit capacitors, despite a slight variation of the value of  $C_{probe}$  due to  
 183 the effect of high permittivities (Eccostock) on the linearity of the regression functions.

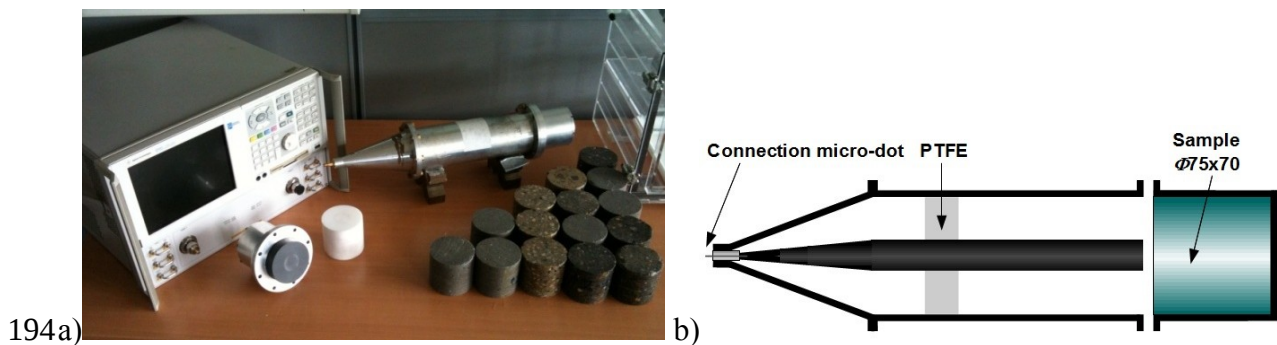
184 This calibrating protocol makes it now possible to determine the real part of the relative  
 185 permittivity (also called dielectric constant) at 33 MHz with capacitive probes.

186

## 1872.2. Coaxial/cylindrical transition line

188The coaxial/cylindrical transition line (also named EM cell) was designed to measure  
189complex dielectric permittivity of civil engineering rough materials at radar frequencies. It  
190consists of a vector network analyzer, which is controlled by a central processing unit and  
191connected to a cylindrical transition line via a coaxial cable [27]. The test sample is placed in  
192a cylindrical waveguide holder connected to the coaxial line (Fig. 4).

193



195Figure 4 : Coaxial/cylindrical transition line (a) EM cell presented with the network analyzer and several  
196concrete samples. (b) Scheme of the coaxial/cylindrical transition line.

197

198The dimensions of the cell ( $\text{Ø}75 \times 70$  mm) correspond to a volume greater than the Elementary  
199Representative Volume of a heterogeneous mixture for a maximal diameter of aggregate  
200 $D_{max} = 20$  mm.

201

202This EM cell enables measuring the permittivity of cylindrical samples of heterogeneous  
203materials with large aggregate dimensions (up to 25 mm) over a frequency range from  
20450 MHz to an upper limit, which depends on the value of the real part of permittivity. This  
205latter frequency limit has been found to equal 800 MHz for all concrete mix formulations in  
206dry conditions, then decreases for saturated concretes displaying high permittivity values.  
207Beyond these values, resonance phenomena disturb the data analysis to a considerable extent.  
208So we consider that the dispersion curve is obtained with confidence between 50 and  
209600 MHz in this study. That is the reason why it is necessary to extrapolate the data obtained  
210by the coaxial/cylindrical transition line on a large frequency bandwidth, at lower and greater  
211frequencies to be able to link the results of all the in situ methods at the correct frequencies.  
212Thereby, the 4p-variant of Jonscher's model [11, 16] constitutes an outstanding means to fit  
213the permittivity dispersion curves on broad frequency bandwidth and to extrapolate the EM  
214cell results at the required low frequency.

215

### 2163. Frequency power law describing the dispersion curve of the complex 217permittivity: inversion-extrapolation procedure

218

#### 2193.1. 4p-variant of Jonscher's model

220Jonscher's model, which is also known as the universal dielectric response, is based on  
221universality in the form of dielectric response. A variant that proved its validity for the EM  
222characterization of concretes on large bandwidth is the four-parameter (4p) variant of  
223Jonscher's model [11, 15]:

$$224 \quad \varepsilon_e(\omega) = \varepsilon_0 \chi(\omega) + \varepsilon_\infty - j \frac{\sigma_{dc}}{\omega} \quad (4)$$

$$225 \text{with} \quad \chi(\omega) = \chi_r \left( \frac{\omega}{\omega_r} \right)^{n-1} \left( 1 - j \cot \left( \frac{n\pi}{2} \right) \right) \quad (5)$$

226

227where  $\varepsilon_\infty$  is the instantaneous dielectric response,  $\sigma_{dc}$  the direct current conductivity,  $\chi_r$  the  
228relative dielectric susceptibility and  $n$  the dispersion parameter,  $\omega$  the angular frequency and  
229 $j = \sqrt{-1}$ . The reference angular frequency  $\omega_r$  is arbitrary chosen.

230 Since the EM cell is limited to the minimum frequency of 50 MHz, while the  
231capacitive technique is valid only around 33 MHz, then we developed a new method to cross  
232the validity ranges of these two techniques. This method is based on the extrapolation of the  
233coaxial/cylindrical transition line data using the 4p-variant of the Jonscher's model.

234

#### 2353.2. Extrapolation method: principle and validation on published data

236Ihamouten et al. [16] showed that 4p-variant reveals no limitation over the whole  
237coaxial/cylindrical transition line frequency range, as it follows accurately the permittivity  
238variations. These results led us to invert the complex permittivity dispersion curve of the EM  
239cell data using the 4p variant of Jonscher's model in order to extract the 4 parameters for a  
240limited bandwidth.

241As observed in (4), the power-law behaviour of experimental data may be concealed by the  
242presence of  $\sigma_{dc}$  in  $\varepsilon_e(\omega)$  at low frequencies and by  $\varepsilon_\infty$  in  $\varepsilon_e(\omega)$  at high frequencies. In theory,  
243both of these disturbing influences can be removed by applying the Kramers–Krönig  
244transformation. Mathematically speaking, the Hilbert transform of a constant is zero; thus,  $\varepsilon_\infty$   
245is not included in the Hilbert transform of  $\varepsilon_e(\omega)$  nor is  $\sigma_{dc}$  included in the transform of  $\omega\varepsilon_e(\omega)$ .

246 These considerations underscore the significance of the Kramers–Krönig transformation in  
 247 the processing and interpretation of experimental data. To this end, we propose herein a  
 248 computationally efficient two-step procedure for estimating the four model parameters. The  
 249 first step consists of estimating the first pair of parameters  $(\chi_r, n)$  from the Hilbert transform  
 250  $H$  of  $\varepsilon_e(\omega)$  and  $\omega\varepsilon_e(\omega)$  via a nonlinear optimization of the following cost function:

$$251 \quad C(\chi_r, n) = \min_{\chi_r, n} \left| \Im \left[ H \left( \varepsilon_e^{model} - \varepsilon_e^{expe} \right) \right] + \Im \left[ H \left( \varepsilon_e'^{model} - \varepsilon_e'^{expe} \right) \right] \right|^2 \quad (6)$$

252 where  $\Im$  and  $H$  denote the imaginary part and the Hilbert transform, respectively. For the  
 253 second step, each of the  $\varepsilon_\infty$  and  $\sigma_{dc}$  terms can be estimated as the solution to a simple linear  
 254 least-squares problem, as follows:

$$255 \quad \varepsilon_\infty = \frac{1}{N} \sum_{i=1}^N [\varepsilon_e'(\omega_i) - \varepsilon_0 \tilde{\chi}'(\omega_i)] \quad (7)$$

$$256 \quad \sigma_{dc} = \frac{\sum_{i=1}^N \omega_i^{-1} [\varepsilon_e''(\omega_i) - \varepsilon_0 \tilde{\chi}''(\omega_i)]}{\sum_{i=1}^N \omega_i^{-2}} \quad (8)$$

257

258 where  $N$  is the number of frequencies and where  $\tilde{\chi}'$  and  $\tilde{\chi}''$  are the estimated real and  
 259 imaginary parts of the susceptibility  $\tilde{\chi}$  (4). The two-step procedure has provided nearly the  
 260 same fitting error and parameter values as the more computationally demanding minimization  
 261 of the following cost function:

$$262 \quad C(\chi_r, n, \varepsilon_\infty, \sigma_{dc}) = \min_{\chi_r, n, \varepsilon_\infty, \sigma_{dc}} \left| \varepsilon_e^{model} - \varepsilon_e^{expe} \right|^2 \quad (9)$$

263

264 For this reason, the two-step procedure is preferred.

265 Using the parameters  $[\chi_r, n, \varepsilon_\infty, \sigma_{dc}]$  extracted from equation (9), we estimate the frequency  
 266 variation of  $\varepsilon_e$  on a large bandwidth using equation (4).

267

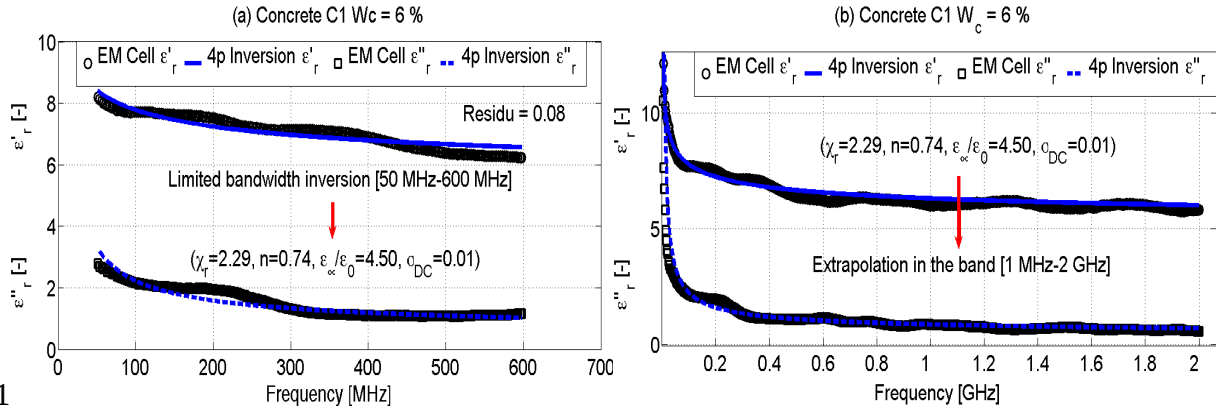
### 268 Extrapolation method validation on published data

269 Since the determination of the complex permittivity of our coaxial/cylindrical transition line is  
 270 limited to the minimum frequency of 50 MHz, we used for this validation published  
 271 experimental data [28], obtained by the EM characterization of two concretes (volumetric  
 272 water content  $W_c = 6\%$  and  $9\%$ ) in the frequency bandwidth [1 MHz-2 GHz].

273 This validation procedure begins with the EM cell data inversion on the band  
 274 [50 MHz- 600 MHz] (Figs 5a and 6a), allowing the extraction of the parameters  $[\chi_r, n, \varepsilon_\infty,$

275  $\sigma_{dc}$ ]. Then we proceed to the rebuilding of the complex permittivity curves on the band  
 276 [1 MHz-2 GHz] with the substitution of the parameters  $[\chi_r, n, \epsilon_\infty, \sigma_{dc}]$  in equation (4) (figures  
 277 5b and 6b). We can see through the results of figures 5a and 6a that the 4p-variant of  
 278 Jonscher's model perfectly fits the experimental data in the case of the two studied concretes,  
 279 although the inversion frequency bandwidth is narrow.

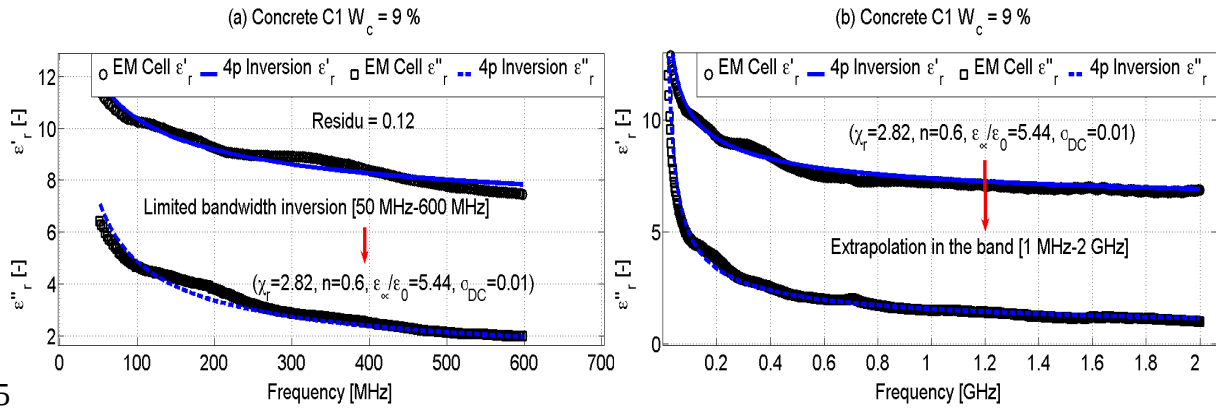
280



281

282 Figure 5: Extrapolation of the EM cell data (concrete C1, water content  $W_c = 6\%$  [26]) from the frequency band  
 283 (a) [50 MHz - 600 MHz] to the frequency band (b) [1 MHz - 2 GHz], using the 4p-variant of Jonscher's model.

284



285

286 Figure 6: Extrapolation of the EM cell data (concrete C1, water content  $W_c = 9\%$  [26]) from the frequency band  
 287 (a) [50 MHz - 600 MHz] to the frequency band (b) [1 MHz - 2 GHz], using the 4p-variant of Jonscher's model.

288

289 The results of figures 5b and 6b show that the broadband extrapolation via this Jonscher's  
 290 model variant perfectly obeys the dielectric behavior of the two concretes, even for very low  
 291 frequencies. This result is also confirmed by the low value of the normalized residues (Figs 5  
 292 and 6) calculated as follow:

293

$$residue = \frac{1}{N} \sum_{i=1}^N \left| \epsilon_{e_i}^{model}(\omega_i) - \epsilon_{e_i}^{expe}(\omega_i) \right|^2 \quad (10)$$

294

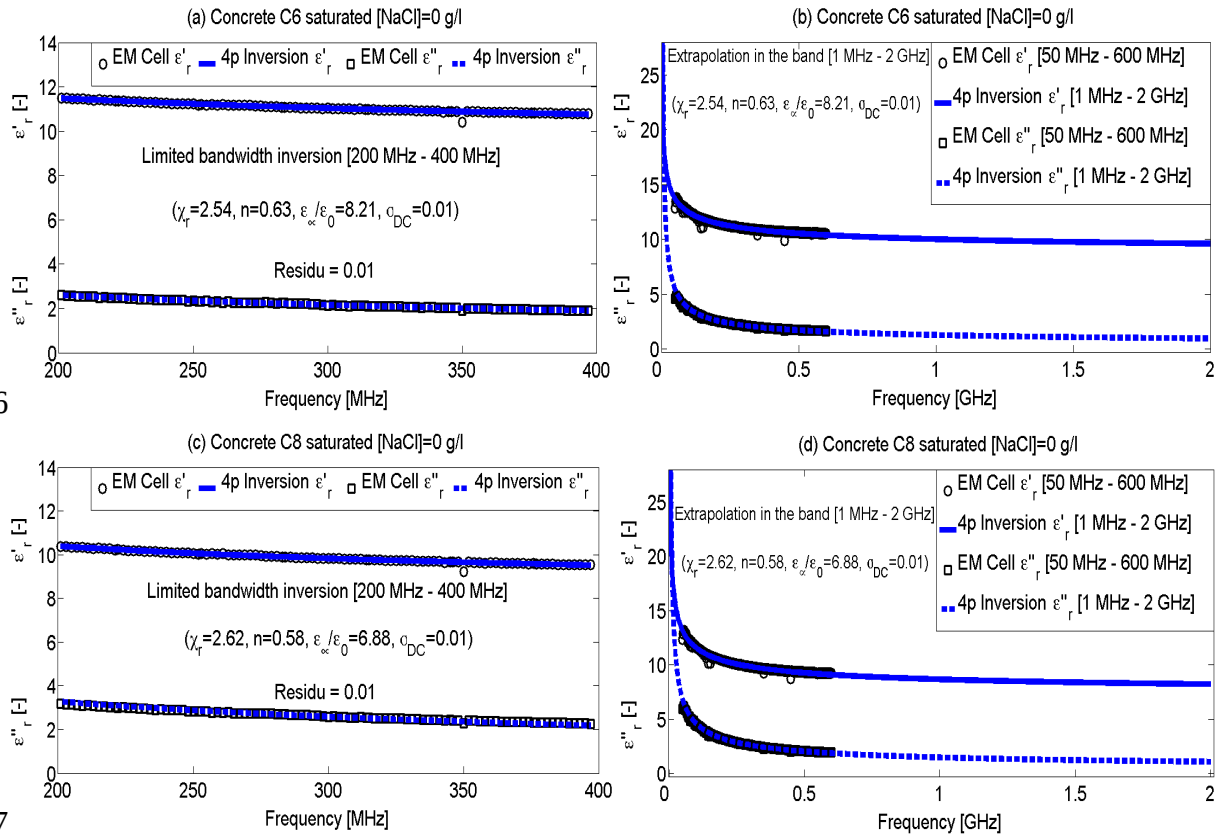
295 To go further in this validation, we tested the sensitivity of this extrapolation procedure in  
 296 front of the low frequency effects of Maxwell-Wagner phenomenon [29]. This phenomenon is  
 297 related to the ionic nature of the concrete interstitial solution. To do this, we applied this  
 298 extrapolation procedure to concrete C6 and C8 (Table 2) presented in detail further in the  
 299 paper.

300

301 Two cylindrical test samples (75×70 mm) corresponding to each of the studied concretes were  
 302 saturated under vacuum [28] with salty water at [NaCl] = 0 g/L and [NaCl] = 120 g/L [20].

303 Figures 7 and 8 include firstly the results of the coaxial/cylindrical transition line  
 304 characterization of the two concretes and secondly, the results of the extrapolation procedure.

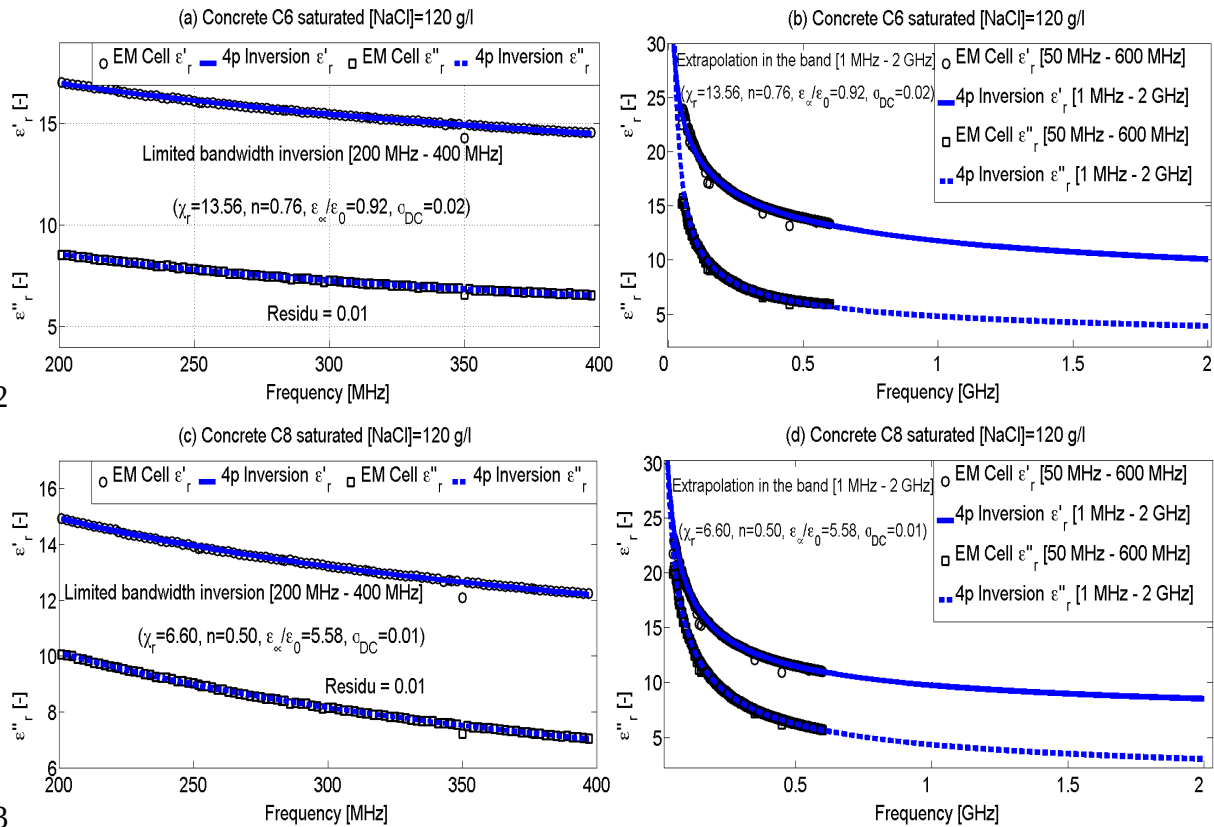
305



307

308 Figure 7: Extrapolation of the EM cell data for concretes C6 (a-b) and C8 (c-d) saturated with water  
 309 [NaCl]=0 g/L from the frequency band [200 MHz - 400 MHz] (a-c) to the frequency band [1 MHz - 2 GHz] (b-  
 310 d), using the 4p-variant of Jonscher's model.

311



312

313

314 Figure 8: Extrapolation of the EM cell data for concretes C6 (a-b) and C8 (c-d) saturated with salt solution  
 315 [NaCl]=120 g/L from the frequency band [200 MHz - 400 MHz] (a-c) to the frequency band [1 MHz - 2 GHz]  
 316 (b-d), using the 4p-variant of Jonscher's model.

317

318 We note that the extrapolation method using the 4p-variant of Jonscher's model allows an  
 319 accurate estimation of the complex relative permittivity in a frequency domain where the  
 320 inversion does not occur to estimate the four parameters, *ie* [50 MHz - 200 MHz].

321 This result demonstrates also the robustness of this method in front of the changes in the  
 322 material characteristics. Indeed, the presence of chloride ions into concrete pore solution in no  
 323 way disturbs the estimation of the complex relative permittivity at low frequencies, despite  
 324 the presence of the effects of the Maxwell-Wagner's phenomena. We can deduce from these  
 325 results that our extrapolation method is able to take into account physical phenomena  
 326 affecting in general the dielectric behavior of concrete.

327

328 In conclusion, the development and the validation of this extrapolation method allow us to  
 329 expand the frequency validity domain of the coaxial/cylindrical transition line measurements.  
 330 This result implies the possibility to compare the EM cell results with those of the capacitive  
 331 probes at the frequencies 33-35 MHz.

332

333

## 3344. Experimental protocol

335

336The six concretes of this study have been originally designed for the electromagnetic  
337characterization of hydraulic concretes through a quadratic experimental design [9]. The  
338composition parameters of the mix design are the nature of the aggregates, the nature of the  
339cement, the cement content, the water to cement ratio ( $W/C$ ) and the quantity of coarse  
340aggregates. The minimum number of concretes, required to obtain the statistically valuable  
341information about these mix parameters, is equal to 36 [9].

342Here, six concretes, made with the same Portland cement and the same proportion of coarse  
343aggregates (Table 2), are selected for the present study. The porosity, measured by water  
344saturation under vacuum [30], is ranging from about 8 to 16%.

345For each concrete, a beam has been cast and, after curing and hardening, sawn into slabs and  
346cored. So, for each mix, we dispose of 3 slabs (300x300x70 mm) for capacitive measurements  
347and 3 cores ( $\varnothing 75 \times 70$  mm) for the EM cell.

348

349Table 2: Concrete mix design and porosity measurement results

| Concrete name | Water to cement ratio | Portland cement*<br>CEM I  | Coarse aggregates<br>(4/20) | Fine aggregates<br>(sand 0/4) | Type of aggregate** | Porosity       |
|---------------|-----------------------|----------------------------|-----------------------------|-------------------------------|---------------------|----------------|
|               | $W/C$ (-)             | ( $\text{kg}/\text{m}^3$ ) | ( $\text{kg}/\text{m}^3$ )  | ( $\text{kg}/\text{m}^3$ )    |                     | (%)            |
| C6            | 0.35                  | 350                        | 1301                        | 715                           | silico-calcareous   | 11.1 $\pm$ 1.4 |
| C8            | 0.35                  | 410                        | 1212                        | 652                           | siliceous           | 10.1 $\pm$ 1.9 |
| C18           | 0.5                   | 350                        | 1192                        | 642                           | siliceous           | 15.0 $\pm$ 3.5 |
| C20           | 0.5                   | 410                        | 1125                        | 619                           | silico-calcareous   | 15.9 $\pm$ 1.7 |
| C30           | 0.55                  | 350                        | 1163                        | 626                           | silico-calcareous   | 15.4 $\pm$ 2.3 |
| C32           | 0.55                  | 410                        | 1074                        | 578                           | siliceous           | 15.8 $\pm$ 2.4 |

350\* Portland cement CEM I 42,5R Anneliese Heidelbergcement Group

351\*\* Siliceous aggregates of Palvadeau, silico-calcareous aggregates of Boulonnais

352

353 As the aim is to study the water content influence, all the samples have been carefully  
354conditioned and controlled. They have been saturated under vacuum then dried at  $T=70^\circ\text{C}$   
355step by step until they reach the mass corresponding to the aimed saturation degrees which are  
356 $S=100\%$ , 75%, 50% and  $\sim 3\%$ . They are then submitted to an homogenization process before  
357non-destructive testing. The homogenization process of the water content is based on Parrott's  
358method [31] which consists in wrapping the sample in tight adhesive aluminium foils and  
359keeping it in the oven during the same time as the drying process duration, so during 2 weeks

360minimum. Note that one slab per aimed saturation degree is used, whereas 2 cylindrical  
361sample per aimed saturation degree are tested, for each concrete.

362 At each step, when the aimed saturation degree is reached and the sample water  
363content distributed homogeneously, the cylindrical samples are tested in the EM cell and the  
364slabs with capacitive probes.

365 At the end of this experimental campaign, all the samples are dried in an oven at  
366105°C to reach a dry state and be able to calculate the real saturation degrees or the real  
367volumetric water content of each step a posteriori according to the standard protocol [30].

368

## 3695. Results and Analysis

370 In this paragraph, the results of the experimental campaign are presented and the  
371extrapolation methodology is applied. Then, the comparison of the measured and extrapolated  
372permittivities makes it possible to validate the methodology.

373

### 3745.1. Capacitive results as a function of the water content

375 Capacitive measurements have been carried out on slabs conditioned in laboratory  
376until they reach a homogeneous saturation degree. The aimed saturation degrees are 100%,  
37775%, 50% and 0% but the results presented here refer always the real volumetric water  
378contents.

379

380 Figure 9 presents the capacitive measurement results obtained on concrete slabs at  
381different water contents. As the dielectric constant is sensitive to the aggregate nature, the  
382results for concretes mixed with silico-calcareous aggregates are separated from the ones  
383mixed with siliceous aggregates. These results show that the dielectric constant is linearly  
384correlated with the volumetric water content in accordance with literature results obtained on  
385other mix designs [20]. We obtained similar results with all the electrode sets. The constant  
386value of the linear regression is smaller for the concretes with siliceous aggregates than for the  
387ones with calcareous aggregates.

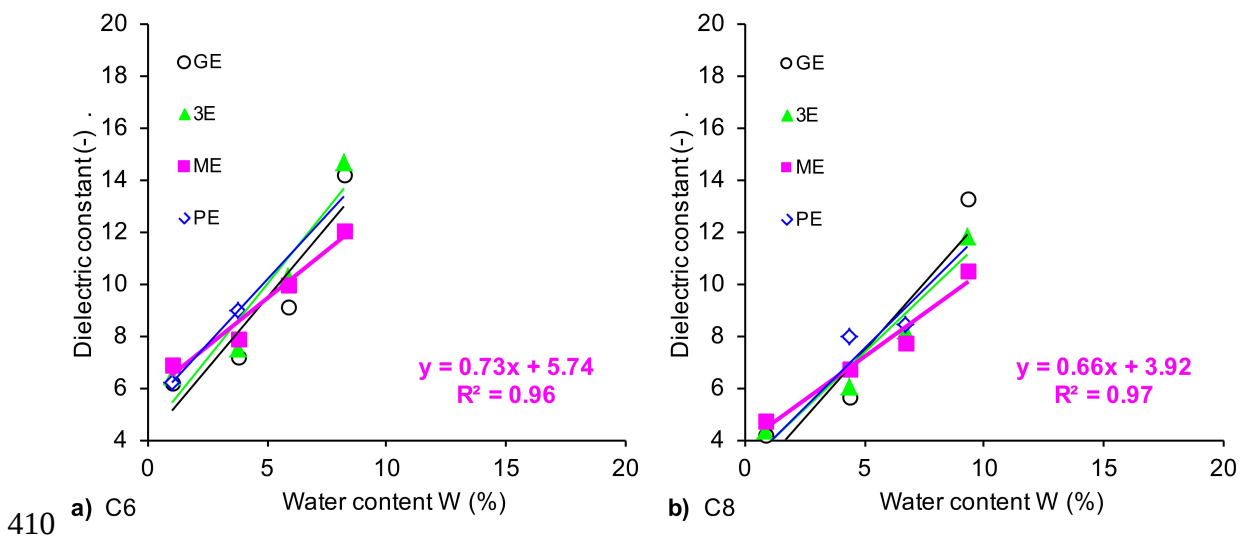
388 Let's note that the variability of the results is mainly due to the material dispersion. It  
389would be reduced by averaging the results on several slabs instead of studying only the mean  
390result on only one slab per aimed saturation degree. Meanwhile the dispersion is relatively  
391small and the regression coefficient valuable.

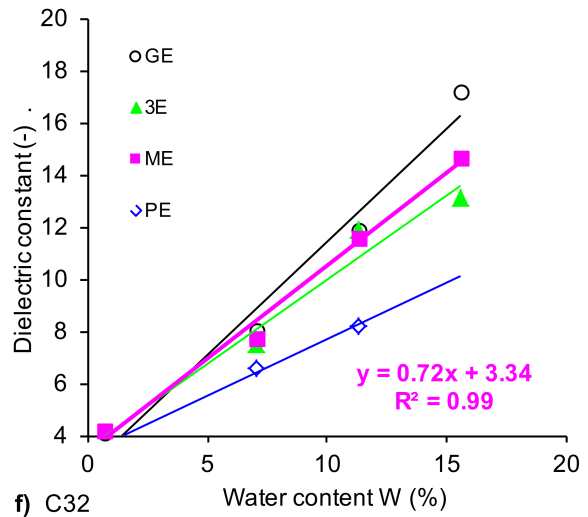
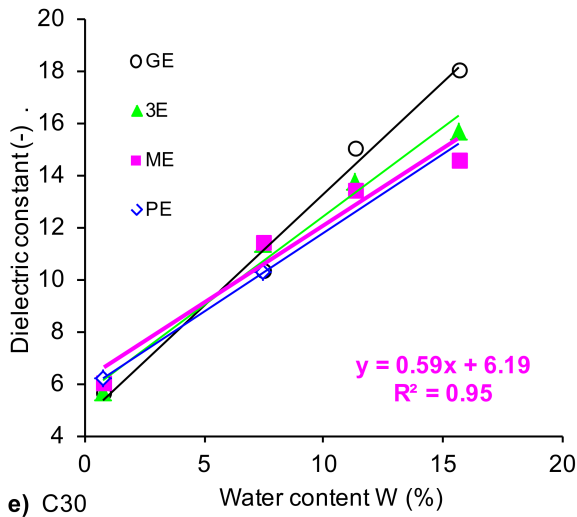
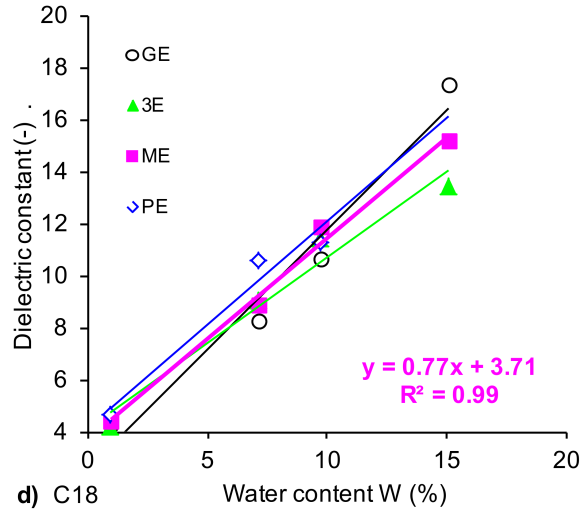
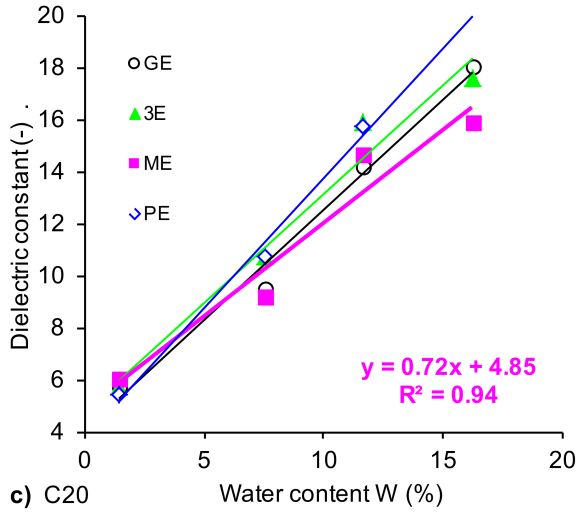
392

### 3935.2. EM Cell results as a function of the water content

394 For the six concretes, two cylindrical samples par mix were studied at four aimed  
 395saturation degrees  $S = 0\%$ ,  $50\%$ ,  $75\%$  and  $100\%$  in the coaxial/cylindrical transition line.  
 396Thus, for each concrete, the tests provided 8 real volumetric water contents and 8 dispersion  
 397curves thanks to the EM cell. An example of dispersion curve for concrete with  $W/C = 0.5$  and  
 398siliceous aggregates is shown in Fig. 1. The other dispersion curves of the complex  
 399permittivity vs frequency obtained are not presented here. They are used to fit the 4p-variant  
 400of the Jonscher's model, between 200 and 400 MHz, which provides thus the extrapolated  
 401complex permittivities at 33 MHz. Fig. 7 shows the results for the concretes C6 and C8 in  
 402saturated conditions.

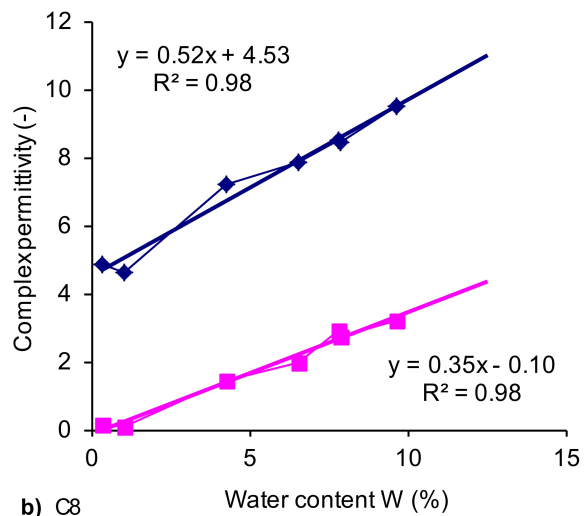
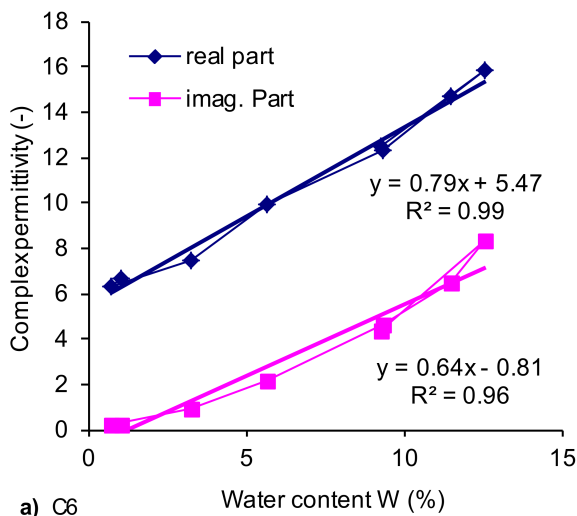
403 Figure 10 gathers the complex permittivity at 33 MHz obtained on concrete cylindrical  
 404samples at different volumetric water contents, for the real and imaginary parts. As in Fig. 9,  
 405the results for concretes mixed with silico-calcareous aggregates are separated from the ones  
 406mixed with siliceous aggregates. As for capacitive probes results, EM cell results show that  
 407the dielectric constant is linearly correlated with the volumetric water content in accordance  
 408with literature results obtained on other mix designs [20] and that the constant of the  
 409regression curve is smaller for mixes with siliceous aggregates.

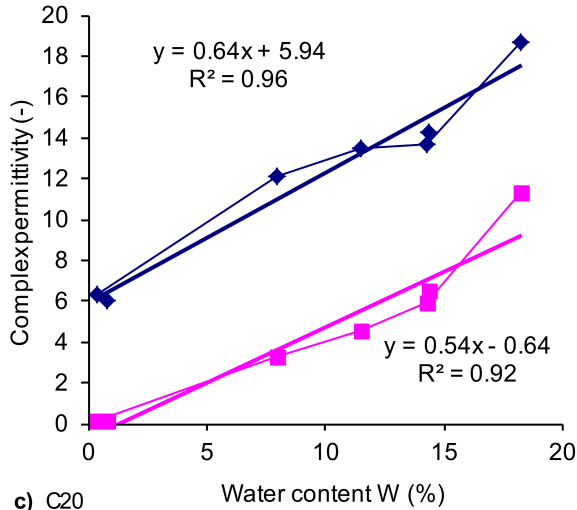




413 Figure 9: Capacitive results on slabs (with 4 electrode sets) function of the volumetric water content – a,c,e)  
 414 Silico-calcareous concretes – b,d,f) Siliceous concretes.

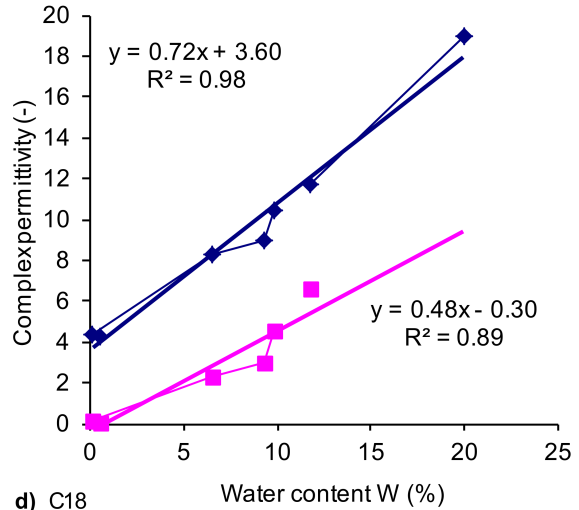
415



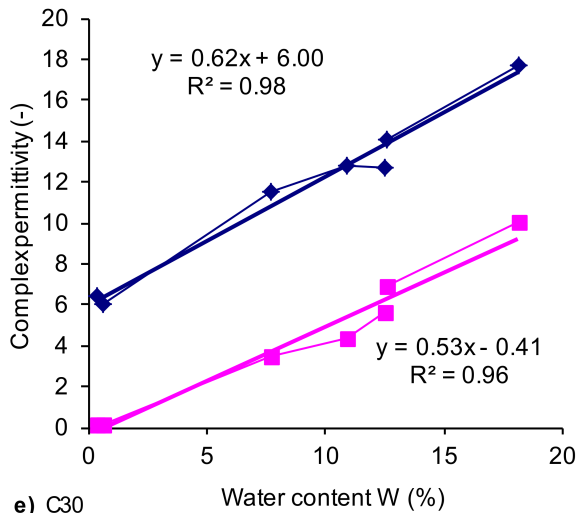


417

c) C20

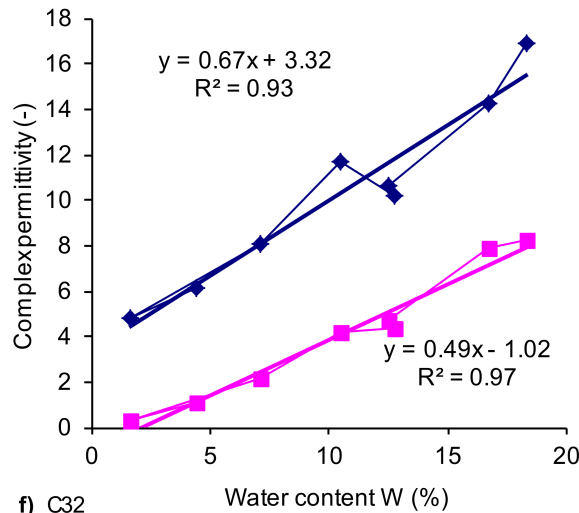


d) C18



418

e) C30



f) C32

419 Figure 10: EM cell results on cores, extrapolated to obtain the complex permittivity as function of the  
420 volumetric water content – a,c,e) Silico-calcareous concretes – b,d,f) Siliceous concretes.

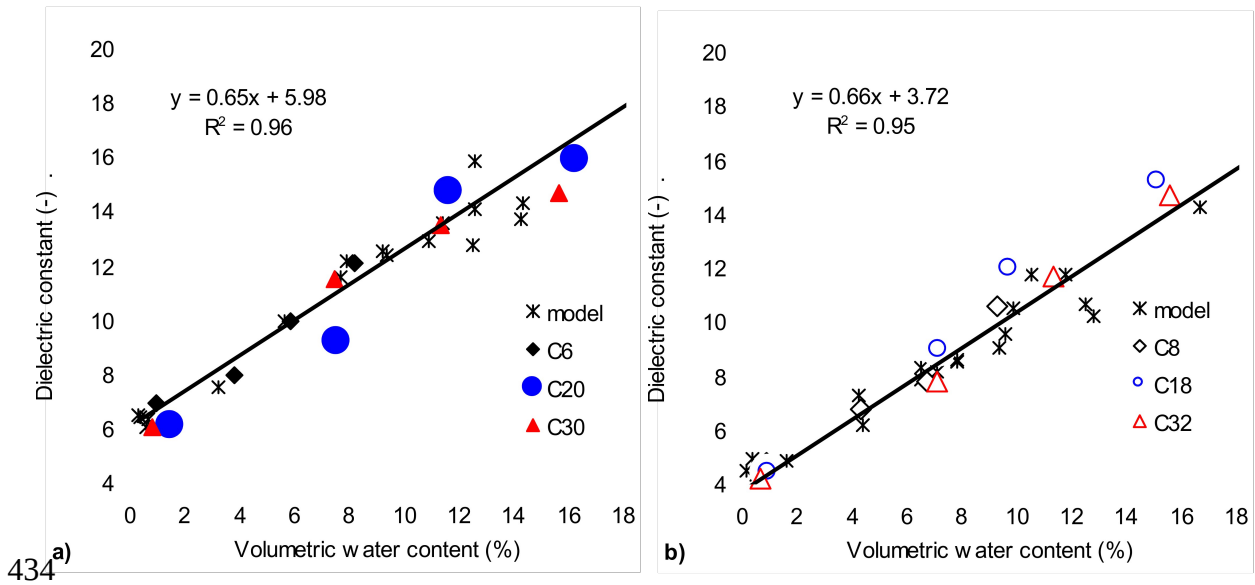
421

### 422 5.3. Comparison between capacitive measurement results and complex permittivity 423 obtained by extrapolation at 33 MHz

424 The 4p-variant of the Jonscher's model was used to fit the dispersion curves of each  
425 concrete cylindrical sample at each water content then they were extrapolated at 33 MHz. The  
426 extrapolated real parts of the complex permittivity at 33 MHz are now compared to the results  
427 of the capacitive probes performed on slabs in similar hydric conditions but not exactly the  
428 same.

429 Figure 11 make it possible to compare these extrapolation results to the capacitive  
430 measurement dielectric constant at 33MHz. We notice that the extrapolated data are plotted  
431 (stars) without making the difference between concrete mixes to simplify the figure. This is

432 possible because only the quantity of cement and the quantity of water varies for these mixes,  
 433 not the nature of the components.



434 a) 435 Figure 11: Comparison of the Jonscher's model extrapolation with the capacitive results at 33MHz – a) Silico-  
 436 calcareous concretes – b) Siliceous concretes

437

438 These figures 11a and 11b show the very good correspondence between all experimental data  
 439 and extrapolated data for each type of aggregate. They also highlight the capability of the 4p  
 440 Jonscher's model to link the results of the both methods studied at low frequency.

441 Tables 4 and 5 show the regression coefficients for every measurement and extrapolation as  
 442 functions of the water content. It is interesting to see through these results that the linear trend  
 443 of the variation of the complex permittivity in function of the water content is always verified  
 444 even after the EM cell extrapolation procedure. Furthermore, the comparison between the  
 445 linear regression parameters of tables 4 and 5 shows that the best matches between the EM  
 446 cell extrapolation data and those of the capacitive probes are obtained, nearly for all  
 447 concretes, using the ME electrodes. The correlations remain excellent, above 95 % with one  
 448 exception (concrete C20), and decrease as the porosity increases. This could be explained by  
 449 the higher variability of the extrapolated measurements when the volumetric water content  
 450 becomes important.

451

452 Table 4: Real and imaginary parts of the complex permittivity  $\epsilon$  at 33 MHz obtained on cores by the EM cell and  
 453 extrapolated with Jonscher's model: linear regressions function of the volumetric water content  $\epsilon = aW + b$

| Concrete name | Real part $\epsilon'$ |              |                          | Imaginary part $\epsilon''$ |              |                          |
|---------------|-----------------------|--------------|--------------------------|-----------------------------|--------------|--------------------------|
|               | Slope $a$             | Constant $b$ | Correlation coeff. $r^2$ | Slope $a$                   | Constant $b$ | Correlation coeff. $r^2$ |
| C6            | 0.79                  | 5.47         | 0.99                     | 0.64                        | -0.81        | 0.96                     |
| C8            | 0.52                  | 4.53         | 0.98                     | 0.30                        | -0.10        | 0.98                     |
| C18           | 0.72                  | 3.60         | 0.98                     | 0.52                        | -0.30        | 0.89                     |
| C20           | 0.64                  | 5.94         | 0.96                     | 0.54                        | -0.64        | 0.92                     |
| C30           | 0.62                  | 6.00         | 0.98                     | 0.53                        | -0.41        | 0.96                     |
| C32           | 0.67                  | 3.32         | 0.93                     | 0.49                        | -1.02        | 0.97                     |

454

455 Table 5: Dielectric constant or real part of the permittivity  $\epsilon$  at 33 MHz obtained on slabs by the 4 different

456 capacitive probes: linear regressions function of the volumetric water content  $\epsilon = aW + b$

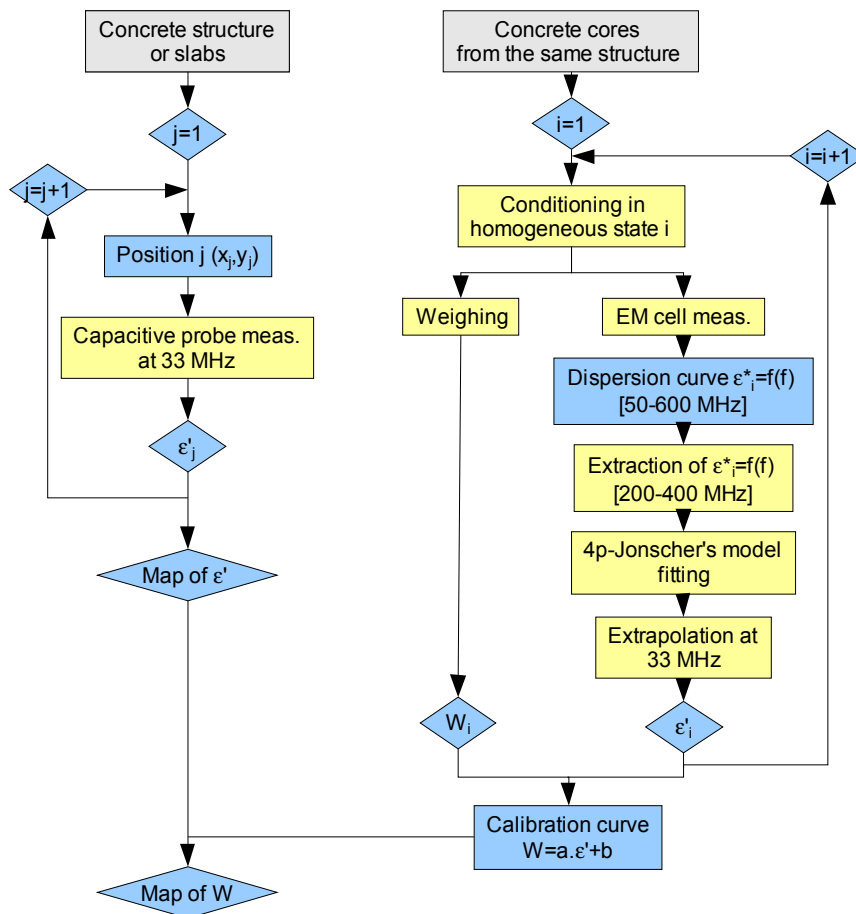
| Concrete name | Electrode size | 33 MHz    |              |                          |
|---------------|----------------|-----------|--------------|--------------------------|
|               |                | Slope $a$ | Constant $b$ | Correlation coeff. $r^2$ |
| C6            | GE             | 1.08      | 4.09         | 0.86                     |
|               | 3E             | 1.14      | 4.33         | 0.91                     |
|               | ME             | 0.73      | 5.74         | 0.96                     |
|               | PE             | 0.99      | 5.19         |                          |
| C8            | GE             | 1.03      | 2.25         | 0.87                     |
|               | 3E             | 0.87      | 2.97         | 0.94                     |
|               | ME             | 0.66      | 3.92         | 0.97                     |
|               | PE             | 0.91      | 2.96         | 0.90                     |
| C18           | GE             | 0.92      | 2.55         | 0.97                     |
|               | 3E             | 0.66      | 4.08         | 0.97                     |
|               | ME             | 0.77      | 3.71         | 0.99                     |
|               | PE             | 0.79      | 4.13         | 0.96                     |
| C20           | GE             | 0.85      | 4.02         | 0.99                     |
|               | 3E             | 0.84      | 4.76         | 0.97                     |
|               | ME             | 0.72      | 4.85         | 0.94                     |
|               | PE             | 1.00      | 3.74         | 0.99                     |
| C30           | GE             | 0.86      | 4.71         | 0.99                     |
|               | 3E             | 0.68      | 6.61         | 0.98                     |
|               | ME             | 0.59      | 6.19         | 0.95                     |
|               | PE             | 0.92      | 4.91         | 0.93                     |
| C32           | GE             | 0.87      | 2.78         | 0.97                     |
|               | 3E             | 0.65      | 3.48         | 0.97                     |
|               | ME             | 0.72      | 3.34         | 0.99                     |
|               | PE             | 0.43      | 3.35         | 1.00                     |

457

458 At this step of the study, we can consider that the coaxial/cylindrical transition line  
459 associated with the Jonscher's extrapolation constitutes a valuable means to obtain the in-lab  
460 calibration curve relating the dielectric constant with the water content on cores before any *in*  
461 *situ* measurements on real structures using the capacitive probes. Let us note also that this  
462 methodology, summarized in the flow-chart of Fig. 12, was employed to get the calibration  
463 curves and to benefit of the capacitive probes ability to determine the dielectric constant at

464 different depths to obtain the water content profiles inside concrete slab in a non-destructive  
 465 way [32, 33].

466



467

468 Figure 12: Flow-chart of the methodology to evaluate and map the water content of a slab or an element of a real  
 469 concrete structure

470

## 4717. Conclusion

472 In this paper, we used the 4p-variant of the Jonscher's model as a means to rely the  
 473 results obtained by two EM testing methods, although their validity ranges are different. An  
 474 extrapolation procedure was developed and validated for the estimation of the complex  
 475 permittivity at very low GPR frequencies. The whole methodology is detailed in this paper.

476 The complex permittivity dispersion curves are determined on cores in a  
 477 coaxial/cylindrical transition line for the characterization of six concrete mixes at four  
 478 different degrees of saturation. In parallel, concrete slabs are conditioned in the same way as  
 479 cores to reach homogeneous degree of saturation, and then tested by the capacitive technique  
 480 using few electrodes of different sizes. The comparison of the capacitive results and the fitted  
 481 dielectric constant is very satisfying.

482 As a consequence, we can consider that the coaxial/cylindrical transition line  
483 associated with the Jonscher's extrapolation constitutes a valuable means to obtain the  
484 calibration curve relating the dielectric constant at 33 MHz with the water content on cores.  
485 For higher frequencies, from 0.8 to 2 GHz, in the GPR frequency range, the same  
486 methodology could be applied to get the calibration curves useful for GPR on site testing in  
487 the same time without extra coring. Thus, as a perspective, the capacitive technique,  
488 combined with GPR in situ measurements, could enable us to accurately characterize cover-  
489 concrete complex permittivities and thus the cover concrete water content or degree of  
490 saturation of a real reinforced concrete structure.

491

## 492 **Acknowledgements**

493 The authors would like to thank the French institute of science and technology for  
494 transport, development and networks (IFSTTAR) and the Ministry of Ecology, Sustainable  
495 Development and Energy for their financial support. We are grateful to want to thank Odile  
496 Coffec (IFSTTAR, site of Nantes) for the technical support she provided.

497

## 498 **References**

- 499[1] Baroghel-Bouny V et al. Concrete design for a given structure service life– Durability  
500 management with regard to reinforcement corrosion and alkali-silica reaction – State  
501 of the art and guide for the implementation of a predictive performance approach  
502 based upon durability indicators, Scientific and technical documents AFGC, Paris,  
503 2007, 252 p.
- 504[2] McCann DM, Forde MC. Review of NDT methods in the assessment of concrete and  
505 masonry structures. *NDT&E International* 2001; 34(2): 71–84.
- 506[3] Robert A. Dielectric permittivity of concrete between 50 MHz and 1 GHz and GPR  
507 measurements for building materials evaluation. *Journal of Applied Geophysics* 1998;  
508 40: 89-94.
- 509[4] Soutsos MN, Bungey JH, Millard SG, Shaw MR, Patterson A. Dielectric properties of  
510 concrete and their influence on radar testing. *NDT&E International* 2001; 34: 419-425.
- 511[5] Laurens S, Balayssac J, Rhazi J, Arliguie G. Influence of concrete relative humidity on  
512 the amplitude of Ground-Penetrating radar (GPR) signal. *Mater Struct* 2002; 35: 198-  
513 203.
- 514[6] Hugenschmidt J, Loser R. Detection of chlorides and moisture in concrete structures  
515 with GPR. *Mater Struct* 2008; 41: 785-792.

- 516[7] Sbartai ZM, Laurens S, Viriyametanont K, Balayssac J-P, Arliguie G. Non-destructive  
517 evaluation of concrete physical condition using radar and artificial neural networks.  
518 Construction and Building Materials, 2009; 23(2): 837-845.
- 519[8] Kalogeropoulos A, van der Kruk J, Hugenschmidt J, Bikowski J, Brühwiler E. Full-  
520 waveform GPR inversion to assess chloride gradients in concrete. NDT & E  
521 International 2013; 57: 74-84.
- 522[9] Dérobert X, Villain G. Development of a multi-linear quadratic experimental design  
523 for the EM characterization of concretes in the radar frequency-band. Construction and  
524 Building Materials, accepted for publication 2016. 24p.
- 525[10] Davis JL, Annan P, Ground-penetrating radar for high-resolution mapping of soil and  
526 rock stratigraphy, Geophys. Prosp., 1989; 37: 531-551.
- 527[11] Bano M. Constant dielectric loss of ground-penetrating radar waves. Geophys J Int  
528 1996; 124: 279-288.
- 529[12] Bois K, Benally A, Nowak P and Zoughi R. Cure-state monitoring and water-to-  
530 cement ratio determination of fresh portland cement based materials using near field  
531 microwave techniques. IEEE Transactions on Instrumentation and Measurement 1998;  
532 47: 628-637.
- 533[13] Bois K, Benally A and Zoughi R. Microwave near-field reflection property analysis of  
534 concrete for material content determination. IEEE Transactions on Instrumentation and  
535 Measurement 2000; 49: 49-55.
- 536[14] Lai WL, Kind T, Wiggenhauser H. Frequency-dependent dispersion of high-frequency  
537 ground penetrating radar wave in concrete. NDT & E International 2011; 44(3): 267-  
538 273.
- 539[15] Lai WL, Kind T, Kruschwitz S, Wöstmann J, Wiggenhauser H. Spectral absorption of  
540 spatial and temporal ground penetrating radar signals by water in construction  
541 materials. NDT & E International 2014;67: 55-63.
- 542[16] Ihamouten A, Chahine K, Baltazart V, Villain G, and Dérobert X. On variants of the  
543 frequency power law for the electromagnetic characterization of hydraulic concrete.  
544 IEEE Transactions on Instrumentation and Measurement 2011; 60(11): 3658-3668.
- 545[17] Ihamouten A, Villain G and Dérobert X. Complex permittivity frequency variations  
546 from multi-offset GPR data: Hydraulic concrete characterization. IEEE Transactions  
547 on Instrumentation and Measurement 2012; 61(6): 1636-1648.
- 548[18] von Hippel A., ed. Dielectric materials and applications. J. Wiley & sons, London  
549 1954. 438 p.

- 550[19] Daniels, D.J., ed. Ground Penetrating Radar. 2<sup>nd</sup> ed, The Institution of Electrical  
551 Engineers. London 2004. 726 p.
- 552[20] Villain G, Sbartaï ZM, Dérobert X, Garnier V, Balayssac JP. Durability diagnosis of a  
553 concrete structure in a tidal zone by combining NDT methods: laboratory tests and  
554 case study. Construction and Building Materials 2012; 37: 893-903.  
555 <http://dx.doi.org/10.1016/j.conbuildmat.2012.03.014>
- 556[21] Villain G, Ihamouten A, du Plooy R, Palma Lopes S, Dérobert X. Use of  
557 electromagnetic non-destructive techniques for monitoring water and chloride ingress  
558 into concrete. Near Surface Geophysics 2015; 13(3): 299-309.
- 559[22] Dérobert X, Villain G, Cortas R, Chazelas JL. EM characterization of hydraulic  
560 concretes in the GPR frequency band using a quadratic experimental design, NDT  
561 Conf. on Civil Engineering In: NDTCE 2009 proceedings, Nantes, France, 2009,  
562 pp.177-182.
- 563[23] Tran NL, Ambrosino R. Mesure de la teneur en eau des sols et des matériaux par une  
564 méthode capacitive: 3—applications de la méthode capacitive de mesure de la teneur  
565 en eau. Bull Pts Ch 1972; 60:173-175.
- 566[24] Dérobert X, Iaquina J, Klysz G, Balayssac JP. Use of capacitive and GPR techniques  
567 for the non-destructive evaluation of cover concrete. NDT & E International  
568 2008;41(1):44-52.
- 569[25] Fares M, Fargier Y, Villain G, Dérobert X, Palma Lopes S. Determining the  
570 permittivity profile inside reinforced concrete using capacitive probes. NDT & E  
571 International 2016; 79: 150-161.
- 572[26] Bore T, Placko D, Taillade F, Himbert M. Capacitive sensor for measuring the filled of  
573 post-tensioned ducts. Experimental set-up, modelling and signal processing. IEEE  
574 Sensors Journal 2013; 13: 457-465.
- 575 [27] Adous M, Quéffélec P and Laguerre L. Coaxial/cylindrical transition line for  
576 broadband permittivity measurement of civil engineering materials. Measurement  
577 Science and Technology 2006; 17: 2241–2246.
- 578[28] Shaari A, Millard S and Bungey J. Modelling the propagation of a radar signal through  
579 concrete as a low-pass filter. NDT&E International 2004; 37:237–242.
- 580[29] Ruffet C, Guéguen Y and Darot M. Complex measurements and fractal nature of  
581 porosity. Geophysics, 1991;56: 758–768.
- 582[30] AFPC-AFREM, Méthodes recommandées pour la mesure des grandeurs associées à la  
583 durabilité, Journées techniques AFPC-AFREM sur la durabilité des bétons, Toulouse–

584 France, 1997.[31] Parrott L. Moisture conditioning and transport properties of  
585 concrete test specimens. *Materials and Structure*, 1994; 27: 460-468.

586[32] Fares M, Villain G, Fargier Y, Thiery M, Dérobert X, Palma Lopes S. Estimation of  
587 water gradient and concrete durability indicators using capacitive and electrical  
588 probes. In: *NDTCE 2015 proceedings*, 2015, Berlin, Germany, p.62-70. [www.ndt.net](http://www.ndt.net)

589[33] Villain G, Sbartai ZM, Lataste J-F, Garnier V, Dérobert X, Abraham O, Bonnet S,  
590 Balayssac J-P, Nguyen NT, Fares M. Characterization of water gradients in concrete  
591 by complementary NDT methods. In: *NDTCE 2015 proceedings*, 2015, Berlin,  
592 Germany, p.448-459. [www.ndt.net](http://www.ndt.net)

593